ADVANCED MATERIALS INTERFACES
Open Access
www.advmatinterfaces.de

Evolution of the Electronic Gap of Directly Synthesized Versus Mechanically Transferred WS_2 Monolayer to Multilayer Films

*Xu He, Jinpeng Tian, Wenjing Wu, Satya Butler, Shengxi Huang, Saien Xie, and Antoine Kahn**

The electronic properties of 2D materials play a critical role in determining their potential for device applications. Despite rapid developments in 2D semiconductors, studies of fundamental electronic parameters, including the electronic gap and ionization energy, are limited, with significant discrepancies in reported values. The study focuses on tungsten disulfide (WS_2) and investigates the electronic structure of films comprising an increasing number of layers deposited with two different methods: direct synthesis via metal–organic chemical vapor deposition (MOCVD) and additive mechanical transfer of exfoliated single layers. The films are characterized via Raman, UV–vis, and photoluminescence spectroscopies, as well as ultraviolet photoelectron and inverse photoemission spectroscopies (UPS/IPES). The electronic gap of WS_2 is found to decrease from 2.43 eV for the monolayer to 1.97 eV for the trilayer, indicating a bulk transition at the trilayer thickness. This reduction in the electronic gap is primarily due to the downward shift of the conduction band minimum relative to the valence band maximum. A comparative analysis with MOCVD-grown WS_2 reveals a slightly larger electronic gap for MOCVD-grown samples, attributed to differences in defect densities. The electronic levels evaluated through UPS/IPES highlight the significant influence of preparation methods on the electronic properties of WS_2.

1. Introduction

Transition metal dichalcogenides (TMD) constitute a class of van der Waals-bonded 2D materials, which have become popular candidates for thin film (opto)electronics given their versatility, superior electrical properties, and tunability of electronic gaps by manipulating composition and number of layers.[1,2] TMD monolayers consist of an X-M-X sandwich formation, where M is a transition metal, such as Mo or W, and X is a chalcogen, including S and Se. With van der Waal forces acting between layers, TMD layers can be stacked in their natural metallic 1T phase, semiconducting 2H phase, or in moiré structures with twisted angles. Unlimited possibilities exist for TMD heterostructure construction because the choice of layers is not bound by lattice matching requirements, a major limiting factor for epitaxial heterostructures of most other non-layered inorganic semiconductors. In recent years, substantial progress[3] has been made in the synthesis, characterization, and application of TMDs, particularly tungsten disulfide (WS_2), from high-quality large-area monolayer growth[4] to novel heterostructures with enhanced optoelectronic properties.[5] The stronger photoluminescence observed from monolayers of WS_2, compared to its counterpart MoS_2, makes this material an ideal candidate for optoelectronics studies.[6,7] The potential of WS_2 in many applications,

X. He, J. Tian, S. Xie, A. Kahn
Department of Electrical and Computer Engineering
Princeton University
Princeton, NJ 08544, USA
E-mail: kahn@princeton.edu

W. Wu
Applied Physics Graduate Program
Smalley–Curl Institute
Rice University
Houston, TX 77005, USA

W. Wu, S. Huang
Department of Electrical and Computer Engineering and the Rice Advanced Materials Institute
Rice University
Houston, TX 77005, USA

S. Butler
Department of Mechanical and Aerospace Engineering
Princeton University
Princeton, NJ 08544, USA

S. Xie
Princeton Materials Institute
Princeton University
Princeton, NJ 08544, USA

The ORCID identification number(s) for the author(s) of this article can be found under https://doi.org/10.1002/admi.202401008

DOI: 10.1002/admi.202401008

including high-performance field-effect transistors,[8,9] sensitive photodetectors,[10,11] efficient catalysts for hydrogen evolution reactions,[12] and valleytronics,[13] is of particular interest to the community.

An exciting aspect of layered 2D materials is how their electronic properties change as a function of the number of layers present in the stack and the distance from the surface or substrate. In that regard, van der Waals-bonded TMDs offer a unique opportunity to test for these changes in a controlled way without affecting the chemistry and bonding of each layer. For this, many studies have been reported for WS_2. However, discrepancies remain surrounding the values for fundamental electronic parameters of WS_2, highlighting the challenges in accurately determining these properties. There are few reports of ionization energy (IE) and electron affinity (EA) of the monolayer WS_2, even though these parameters are crucial for properly evaluating interface electronic structures and essential for predicting band alignment type at heterostructures. Published IE values are found to be inconsistent among themselves: experimentally, 5.74 eV,[20] or theoretically, 5.26,[16] 5.48, and 5.82 eV.[21] Even scarcer and more widely spread are the reported values of exciton binding energies, ranging from 0.32[17] to 0.65[19] and 0.71 eV.[18,22] To the best of our knowledge, there is no experimental report on the EA of WS_2. The energy gap of monolayer WS_2 is the most commonly cited electronic property of the material but has seen considerable variations in reported values across both theoretical and experimental studies, from ≈1.6 to 3.11 eV.[6,14–19] While some variations in energy gap values reported from experimental studies can be attributed to film preparation and quality, measurement techniques, the number of layers probed, or the impact of the substrate on the structural and electronic properties of the film, a fundamental reason behind these variation is the lack of distinction between single-particle (or electronic) gap (E_G) and optical gap (E_{opt}) in literature reports. E_G represents the energy difference between an uncorrelated hole at the valence band maximum (VBM) and an electron at the conduction band minimum (CBM), while the optical gap, often determined through UV–vis spectroscopy, corresponds to the energy required to excite an electron-hole pair, the exciton. This energy is lower due to electron-hole Coulomb interaction, i.e., the exciton binding energy. This distinction is critical for accurate energy level alignment in device applications. Because of the 2D nature of these materials, electron-hole interactions are strong (exciton binding energies are high), and the direct determination of E_G, including the VBM and CBM energy positions, requires two independent techniques, i.e., direct (for VBM) and inverse (for CBM) photoemission spectroscopies. As no systematic experimental work has been reported so far to study the evolution of the electronic properties of WS_2 as a function of the number of layers stacked in the film, we investigate the E_G, IE, and EA of WS_2 films comprising one to multiple layers, using ultraviolet photoelectron spectroscopy (UPS) and inverse photoemission spectroscopy (IPES). This is the first set of direct measurements of frontier energy levels of WS_2 for a different number of layers and provides an experimental benchmark for theoretical calculations. We also contrast results obtained from one- to four-layer films stacked by mechanical transfer with one- to multiple-layer (≥4 layers) films directly synthesized via metal–organic chemical vapor deposition (MOCVD), studying the impacts of preparation methods on the electronic properties of the material.

2. Results and Discussion

2.1. Mechanically Transferred 1L, 2L, 3L, and 4L WS_2

Monolayer (1L), bilayer (2L), trilayer (3L), and tetralayer (4L) WS_2 were mechanically transferred (see methods below) on fused silica, and optical measurements were conducted to test the quality of the layers. The monolayers are stacked in a hexagonal lattice arrangement (2H) with the sulfur and tungsten atoms in a trigonal prismatic arrangement (**Figure 1a**). Photoluminescence (PL) measurements (Figure 1b) show a strong peak for the 1L film at 630 nm (1.97 eV), which reduces in intensity by almost 14-fold for the 2L film and finally to negligible intensities for 3L and 4L films. This is consistent with the reported characteristic transition of several other TMD materials besides WS_2, including MoS_2, $MoSe_2$, and WSe_2, from a direct gap for 1L to an indirect gap for multilayer films.[2,23–27] UV–vis measurements (Figure 1c) show a 620 nm (2.0 eV) peak of exciton A for the monolayer and a 518 nm (2.39 eV) peak for exciton B, a difference due to spin-orbit splitting of the valence band and the doubly degenerate conduction band at the *K* point of the Brillouin zone.[15,16,24,28] As the absorbance increases with an increasing number of layers, as expected from the increasing amount of materials present, there is no significant change to the position of Exciton A or B across the UV–vis measurement for 1L, 2L, 3L, and 4L, consistent with prior reports. Calculations have reported on this layer independence[2,15,23,29] for the excitons because the conduction band states at the *K* point of the Brillouin zone are mostly the result of strongly localized *d* orbitals of the transition metal *W* atoms, and the direct gap at this point changes as little as 0.1 eV for MoS_2[2] or WS_2.[24] Note that the difference between the A exciton peak position (620 nm) and the PL peak position (630 nm) is due to the Stokes shift and effects of strain in the material, as reported by Zhao et al.[25] and Jeong et al.[30] Raman spectroscopy measurements (Figure 1d–f) show a strong second-order longitudinal acoustic 2LA(M) mode peak at ≈351 cm^{-1} superimposed on the peaks of the first-order modes at the Brillouin zone center E^1_{2g} at ≈356 cm^{-1}. The $A_{1\ g}$ peak, which corresponds to a symmetric out-of-plane sulfur vibration, shifts from 417.9 cm^{-1} for 1L to 421 cm^{-1} for the multi-layer films as a result of interlayer interaction. A detailed fitting of the E^1_{2g} and $A_{1\ g}$ peaks, including peak positions for all mechanically transferred and MOCVD films, are presented in Figure S1 and Table S1 (Supporting Information). The spectra are characteristic of WS_2 and present an increase in the E^1_{2g}- $A_{1\ g}$ peak distance, consistent with reported Raman measurements for an increasing number of layers due to the dielectric screening of the vibration modes.[31]

To gain insight into the evolution of the energy levels and electronic gap with the number of layers, we performed UPS/IPES measurements in ultra-high vacuum on mechanically transferred 1L, 2L, 3L, and 4L WS_2 on p-Si substrates with a native oxide (≈1 nm). As shown in **Figure 2**, the positions of the valence band maximum (VBM) and conduction band minimum (CBM) with respect to the vacuum level (E_{vac}) of each film are determined by taking the intersection between the linear

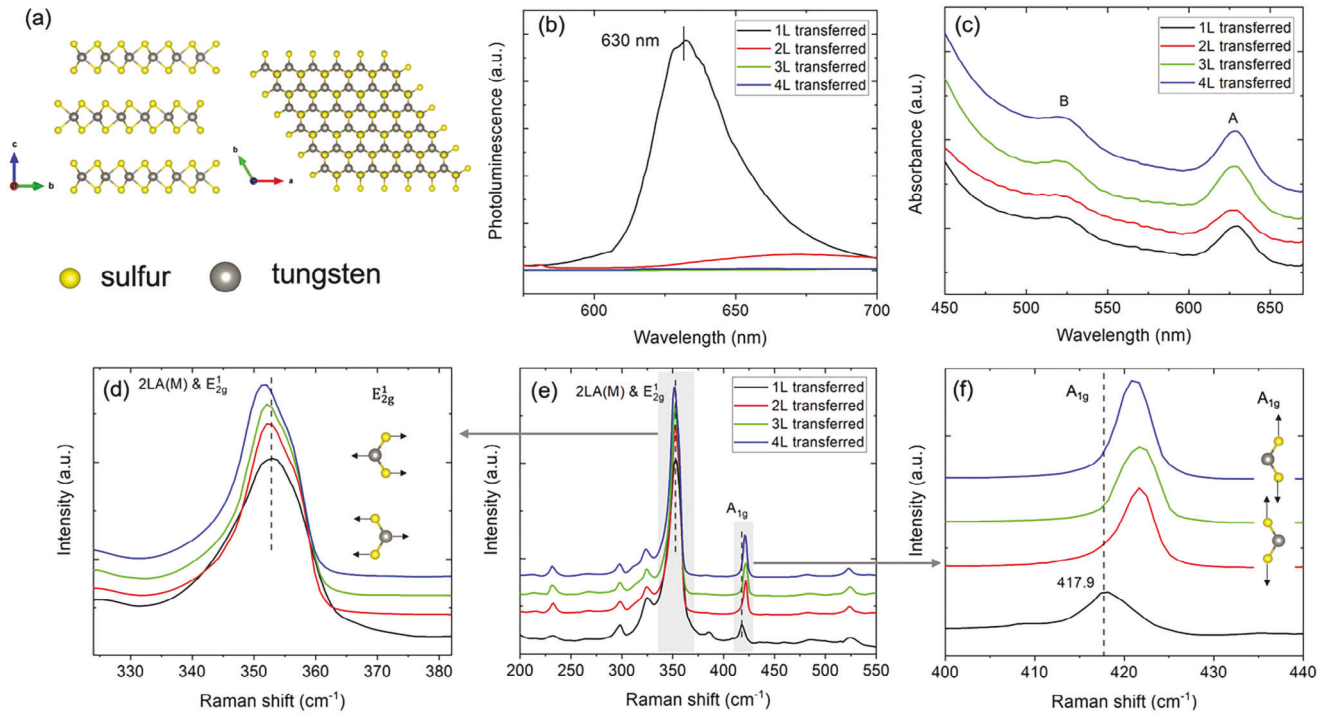

Figure 1. a) Structure of WS_2; b–f) the sequence of data obtained from 1L (black), 2L (red), 3L (green), and 4L (blue) films mechanically transferred on fused silica: (b) photoluminescence, (c) UV–vis absorption, (e) Raman spectroscopy with spectra normalized to E^1_{2g} peak and arbitrarily shifted for clarity; (d) and (f) Expanded views of the E^1_{2g} and $A_{1\ g}$ peaks, respectively.

extrapolation of the leading edge of the valence and conduction state spectra and the background. The detailed fitting for all mechanically transferred films is shown in Figure S2 (Supporting Information). We thus determine E_G = CBM–VBM. We find that E_G of the mechanically transferred and stacked WS_2 decreases from 2.43 eV for the monolayer, to 2.19 eV for the bilayer, and stays at ≈2.0 eV for the trilayer and tetralayer, indicating that the bulk value, as measured by UPS/IPES, is reached between 3L and 4L stacked layers. The resolution of the electronic gap is estimated at ± 0.15 eV based on the experimental resolution of the techniques and reproducibility of data collected from two sets of data for each type of film. A value of E_G equal to 2.43 eV for the mechanically transferred monolayer is consistent with the fitted quasiparticle gap of 2.41 eV by Chernikov et al.[17]

According to our UPS/IPES measurements (Figure 2), the reduction of E_G from monolayer to bulk (or 4L) corresponds primarily to an increase in EA as the CBM shifts away by 0.37 eV from E_{vac}, whereas the VBM shift toward E_{vac} by only 0.08 eV, a relatively small decrease. Most of the increase in EA occurs

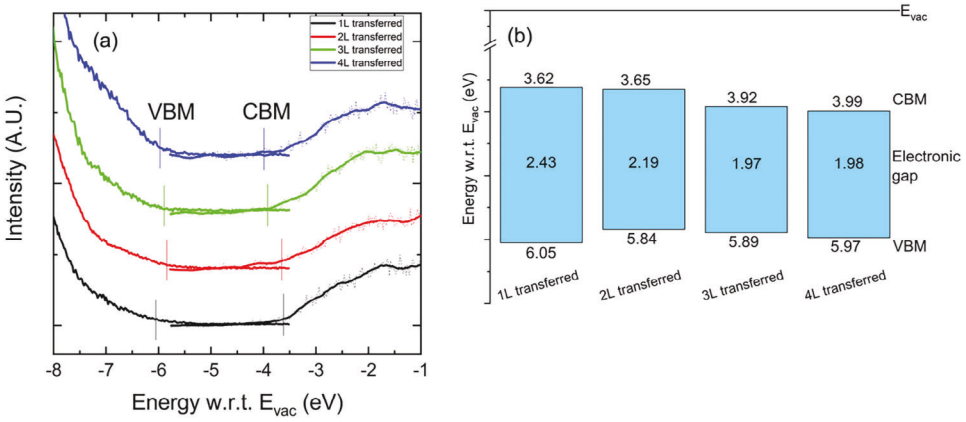

Figure 2. a) combined UPS/IPES spectra of mechanically transferred 1L, 2L, 3L, and 4L WS_2 on p-Si substrates. The leading edges of the valence band are arbitrarily amplified, and the spectra offset for clarity; b) Corresponding energy diagrams showing the evolution of the ionization energy, electron affinity, and electronic gap from a single layer to multilayers. The resolution of the electronic gap is ±0.15 eV.

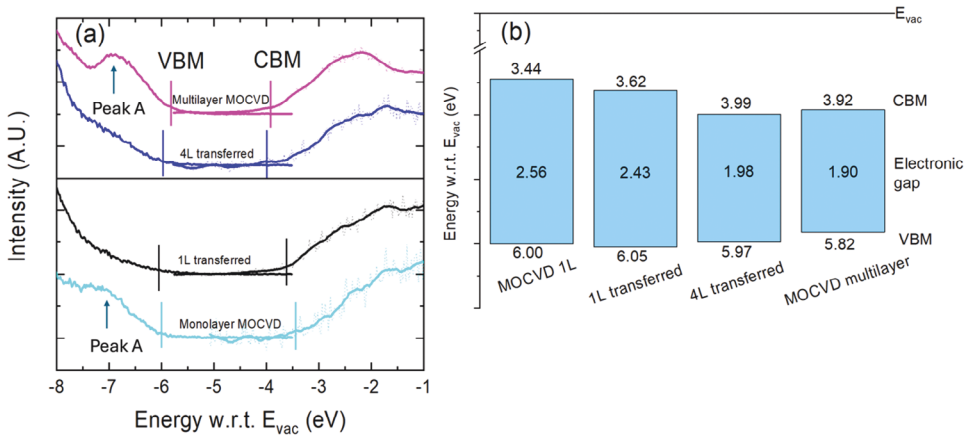

Figure 3. Comparison between a) UPS and IPES spectra and b) electron affinity, ionization energy, and electronic gap of mechanically transferred and MOCVD-grown monolayers and multilayers (or 4L). The resolution of the electronic gap is ±0.15 eV.

between the bilayer (3.65 eV) and the trilayer (3.92 eV) films. It remains largely unchanged (3.62–3.65 eV) between the monolayer and bilayer films, whereas the IE decreases by 0.2 eV in that interval. This is in accord with theoretical calculations by Kuc et al.,[24] which predict that the CBM stays at the *K* point of the Brillouin zone from 1L to 2L WS_2, while the VBM shifts from the *K* point (direct gap) to the Γ point (indirect gap), marking the largest difference in IE in the series. Based on a detailed theoretical investigation of MoS_2 (1L–6L), Mak et al.[2] postulated that such a shift is driven by perpendicular quantum confinement (or decrease thereof when adding layers to the stack). According to Kuc et al.,[24] the larger increase in EA occurs between bilayer and trilayer (or tetralayer) as the CBM position shifts from the *K* point valley to a valley point between the Γ and *K* points, while IE stays essentially unchanged because the VBM remains on the same valley going forward. Naik et al.[32] attributed this transition to a change in hybridization as the CBM states along the Γ-*K* direction and VBM states at Γ are more delocalized in the out-of-plane direction due to their strong sulfur p_z orbital presence, leading to a greater hybridization with other layers than at the K point and hence a larger band splitting at the bilayer-trilayer transition.

2.2. Directly Synthesized Versus Mechanically Transferred WS_2

To investigate the impact of preparation methods on the electronic properties of WS_2, we compare films made by direct synthesis via MOCVD growth with those stacked via mechanical transfer. The E_G of the MOCVD-grown WS_2 monolayer is 2.56 eV (see **Figure 3**), slightly larger than that of the mechanically transferred monolayer. This trend is observed again with the optical gap (E_{opt}) measured by UV–vis absorption (**Figure 4a**), which shows a slightly red-shifted absorption peak for the mechanically transferred layer (620 nm) compared to the MOCVD-grown layer (616.6 nm). This trend is also evident in the PL spectrum (Figure 4b), which peaks at 1.97 eV (630 nm) for the mechanically transferred layer and 1.99 eV (624 nm) for the MOCVD-grown monolayer. The difference in the gap between transferred and MOCVD-grown films decreases as the number of layers increases: the electronic gap measured on the MOCVD-grown multilayer is 1.90 eV, consistent with that of the mechanically transferred WS_2 (≥3 layers). The full energy level diagrams of MOCVD-grown 1L and multilayer films and mechanically transferred 1L, 2L, 3L, and 4L films are shown in Figure S3 (Supporting Information).

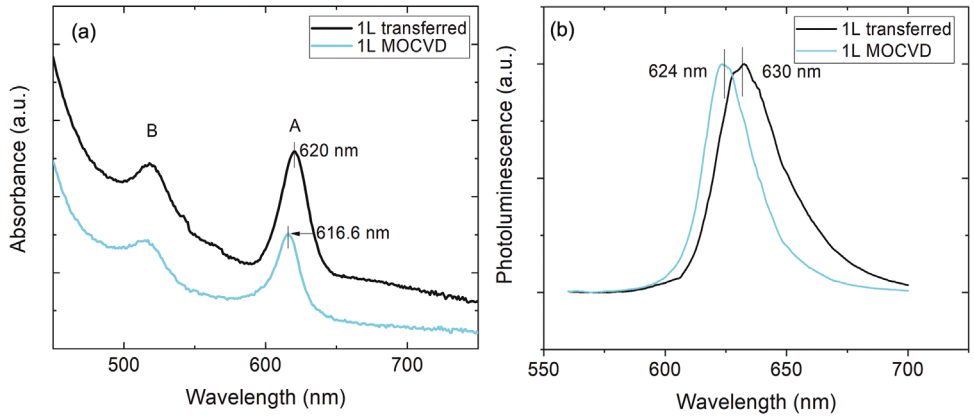

Figure 4. a) UV–vis spectra, and b) normalized photoluminescence of mechanically transferred 1L (black) and MOCVD-grown 1L (cyan).

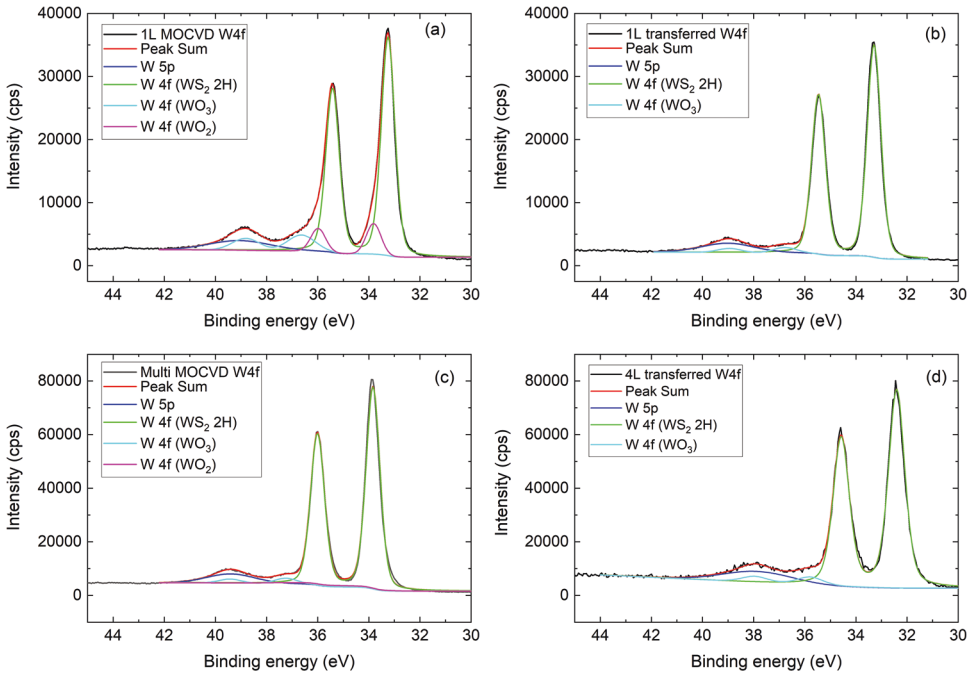

Figure 5. a,b) XPS fitting of W 4f for MOCVD-grown and transferred monolayers, c) MOCVD-grown multilayers, and d) mechanically transferred 4L with W 5p (blue), W 4f of 2H-WS_2 (green), WO_3 (cyan), and WO_2 (magenta).

We note that the MOCVD-grown WS_2 exhibits a photoemission feature at ≈1 eV below the VBM (Peak A), which is far less prominent in the spectra of the mechanically transferred material (Figure 3a). This feature is likely related to the band structure of the TMD at the Γ-point and is clearly observable in our angle-integrated photoemission experiments on films grown directly by MOCVD, which are polycrystalline and present multiple azimuthal orientations. On the other hand, the assembly of mechanically transferred layers presents a single orientation, which may or may not be in alignment with the specific measurement angle of our spectrometer, thereby leading to a less defined feature.

To further understand the difference in E_G between MOCVD-grown and mechanically transferred films, detailed X-ray photoemission spectroscopy (XPS) scans of the *W 4f* core level peaks were taken, and their respective fitting is shown in **Figure 5**. Survey scans of all the films were also collected and are included in Figure S4 (Supporting Information). The analysis shows components of *W 4f* corresponding to *W* bonded to sulfur (WS_2) and oxygen (WO_3) on all multilayers and monolayers prepared by both methods, although the oxide component is clearly stronger in the MOCVD-grown films. In addition, the MOCVD-grown films, especially at the monolayer level, have a non-negligible contribution from a *W 4f* doublet shifted by 2.85 eV toward lower binding energy from the commonly seen WO_3 peak, which can be attributed to the presence of WO_2.[33] Also present in all spectra is a *W 5p* component. The oxide-related core levels indicate the presence of more oxygen-related defects and, hence, show less tungsten bonded to sulfur in the MOCVD-grown monolayer: the ratio of tungsten (bonded to sulfur) to sulfur (W:S ratio) is 0.42 for the MOCVD monolayer, lower than 0.45 for the mechanically transferred 1L. The W:S ratio of the MOCVD-grown multilayer film is 0.48, closer to the 0.49 ratio of the mechanically transferred 4L film, indicating a similar film quality for multilayers. Hence, a 0.13 eV difference in E_G in the monolayers of two preparation methods can be explained by the difference in film quality, as defined here as the closeness of W:S ratio to 0.5, which increases as the number of layers increases, evidenced by the much smaller difference of 0.08 eV in E_G for multilayer-4L films, with a minor contribution from different film strain[30] as evidenced by the small PL peak redshift in Figure 4b.

In addition, the intensity of the W4f detailed scans allows us to follow the number of WS_2 layers in the films. In particular, the analysis provides a lower bound of four layers comprised in the MOCVD multi-layer films, which is consistent with the fact that the electronic gap of that film is about equal to that of the 4L mechanically transferred one, as shown in Figure 3. The details of the analysis are given in Supporting Information and Figure S5 (Supporting Information).

Finally, the data presented here provide an opportunity to evaluate the exciton binding energy (E_B) in the 1L films. Taking the difference between electronic gaps (E_G) given in Figure 3b and optical gaps (E_{opt}) given in Figure 4a, E_B is evaluated at 0.55 eV for the MOCVD-grown monolayer and 0.43 eV for the mechanically transferred monolayer. This large exciton binding energy can be expected given the quantum confinement in these 2D layers and the weak dielectric screening effect[17] from the silicon oxide substrate, leading to a strong Coulomb interaction in the excited electron-hole pair.

3. Conclusion

In this work, the electronic properties of WS_2 layers, as characterized by UPS/IPES, reveal a notable decrease in the electronic

gap with increasing layer thickness, from 2.43 eV in monolayers to 1.97 eV in trilayers, signaling a bulk electronic structure starting at the trilayer. These results fill the gap of the lack of experimental data on essential electronic properties parameters, including IE, EA, and E_G, for WS_2 materials. The electronic gap reduction is predominantly due to the CBM shifting away from the vacuum level, with a minimal shift in the VBM. This series of direct measurements of energy levels and the electronic gap provides important guidelines for designing TMD-based optical and electronic devices, which requires a good match of energy levels, particularly at interfaces. Comparisons with MOCVD-grown WS_2 highlight the impact of preparation methods on material properties. There are slight variations in electronic gap and exciton binding energies. The discrepancy in energy levels between MOCVD-grown and mechanically transferred samples could be attributed to the fewer defects in the mechanically transferred samples, according to detailed XPS studies. The difference between the electronic properties of WS_2 prepared by mechanical exfoliation and MOCVD growth decreases as the layer number increases.

4. Experimental Section

Film Preparation: Two different film-fabrication methods, MOCVD and mechanical transfer, were utilized. The mechanical transfer method[34] uses an ultra-flat gold tape created through a template-stripping technique. A thin gold film was evaporated on a polished silicon wafer (Nova Electronics) and then stripped off with thermal release tape after spin-coating a polyvinylpyrrolidone (PVP) layer. This gold tape exfoliates a monolayer from the WS_2 crystal purchased from HQ Graphene, which was then transferred onto a desired substrate or existing layer to stack more layers of WS_2. The thermal release tape and PVP layer were removed, and the gold was etched away with an iodine solution, yielding large-area monolayers. WS_2 films with 1L, 2L, 3L, and 4L were constructed in ABAB stacking order (2H phase) on fused silica for optical measurements (PL, Raman, and UV–vis) and p-Si substrates with a native oxide for UPS, IPES, and XPS.

For the MOCVD growth method, monolayer and multilayer films of continuous coverage were grown directly on p-Si substrates with native oxide. Tungsten hexacarbonyl (THC) and diethyl sulfide (DES) mixed with Ar carrier gas were used as the precursor for tungsten and sulfur, respectively. Monolayer (or multilayer) WS_2 films were grown under a total pressure of ≈1.7 Torr, at a growth temperature of 600 °C for 3 h, with flow rates of 2 (or 10) sccm for THC, 0.5 sccm for DES, 1 sccm H_2, and 350 sccm Ar.

Characterization: Photoluminescence (PL) and Raman spectroscopy were used to distinguish monolayers from multilayers. The measurements were performed on a Horiba Raman Spectrometer with a 532 nm laser. The nominal laser power was attenuated with a filter D2 for Raman measurements and D0.3 for PL measurements to prevent detection saturation. UV–vis spectroscopy (UV–vis) was used in conjunction to measure the optical gap (E_{opt}), which aids in the calculation of exciton binding energy for monolayer WS_2 materials.

Combined ultraviolet photoelectron spectroscopy (UPS) and inverse photoemission spectroscopy (IPES) were used to probe the material's occupied and unoccupied states, determine the conduction band minimum (CBM), valence band maximum (VBM), electron affinity (EA), ionization energy (IE), and electronic gap (E_G) as a function of the number of layers. Both UPS and IPES were performed in an ultra-high vacuum (10^{-10} Torr). UPS utilized He I photons (21.22 eV) generated by a helium discharge lamp, with a pass energy of 5 eV, a 0.02 eV step size, while IPES was performed in isochromatic mode with electron energies ranging from 5 to 15 eV.

X-ray photoelectron spectroscopy (XPS) with a monochromated Al K-α anode (1486.6 eV) by Thermo Fisher Scientific was used to probe the W 4f and S 2p core levels. Scans were taken with a pass energy of 25 eV and a 0.05 eV step size with a base pressure ≈10^{-7} Torr.

Supporting Information

Supporting Information is available from the Wiley Online Library or from the author.

Acknowledgements

Work in Princeton was supported in part by a grant from the Department of Energy Office of Basic Energy Science, Division of Materials Sciences and Engineering under Award #DE-SC0012458, and by the Eric and Wendy Schmidt Transformative Technology Fund. The authors acknowledge the use of Princeton's Imaging and Analysis Center (IAC), which was partially supported by the Princeton Center for Complex Materials (PCCM), a National Science Foundation (NSF) Materials Research Science and Engineering Center (MRSEC; DMR-2011750). W.W. and S.H. acknowledge the funding support from NSF (ECCS-2246564, ECCS-1943895) and Air Force Office of Scientific Research (AFOSR) under grant FA9550-22-1-0408.

Conflict of Interest

The authors declare no conflict of interest.

Data Availability Statement

The data that support the findings of this study are available from the corresponding author upon reasonable request.

Keywords

2D materials, energy gap, layer-dependent properties, photoemission spectroscopy, tungsten disulfide

Received: December 17, 2024
Revised: February 10, 2025
Published online:

[1] Q. H. Wang, K. Kalantar-Zadeh, A. Kis, J. N. Coleman, M. S. Strano, *Nat. Nanotechnol.* **2012**, *7*, 699.
[2] K. F. Mak, C. Lee, J. Hone, J. Shan, T. F. Heinz, *Phys. Rev. Lett.* **2010**, *105*, 136805.
[3] C. Lan, C. Li, J. C. Ho, Y. Liu, *Adv. Electron. Mater.* **2021**, *7*, 2000688.
[4] Y. Gao, Z. Liu, D. M. Sun, L. Huang, L. P. Ma, L. C. Yin, T. Ma, Z. Zhang, X. L. Ma, L. M. Peng, H. M. Cheng, W. Ren, *Nat. Commun.* **2015**, *6*, 8569.
[5] C. Zhang, C. P. Chuu, X. Ren, M. Y. Li, L. J. Li, C. Jin, M. Y. Chou, C. K. Shih, *Sci. Adv.* **2017**, *3*, e1601459.
[6] H. R. Gutiérrez, N. Perea-López, A. L. Elías, A. Berkdemir, B. Wang, R. Lv, F. López-Urías, V. H. Crespi, H. Terrones, M. Terrones, *Nano Lett.* **2013**, *13*, 3447.
[7] N. Peimyoo, W. Yang, J. Shang, X. Shen, Y. Wang, T. Yu, *ACS Nano* **2014**, *8*, 11320.
[8] D. Ovchinnikov, A. Allain, Y. S. Huang, D. Dumcenco, A. Kis, *ACS Nano* **2014**, *8*, 8174.

[9] L. Jin, J. Wen, M. Odlyzko, N. Seaton, R. Li, N. Haratipour, S. J. Koester, *ACS Omega* **2024**, *9*, 32159.
[10] N. Perea-Lõpez, A. L. Elías, A. Berkdemir, A. Castro-Beltran, H. R. Gutiérrez, S. Feng, R. Lv, T. Hayashi, F. Lõpez-Urías, S. Ghosh, B. Muchharla, S. Talapatra, H. Terrones, M. Terrones, *Adv. Funct. Mater.* **2013**, *23*, 5511.
[11] V. K. Pulikodan, M. Raees A, A. Alexander, A. K. Nalledath, M. A. G. Namboothiry, *ACS Appl. Nano Mater.* **2024**, *7*, 8007.
[12] L. Xia, K. Pan, H. Wu, F. Wang, N. Zhao, H. Yu, Y. Ren, M. Chang, Z. Dong, S. Wei, *J. Phys. Chem. Solids* **2024**, *184*, 111708.
[13] B. Zhu, H. Zeng, J. Dai, Z. Gong, X. Cui, *Proc. Natl. Acad. Sci. USA* **2014**, *111*, 11606.
[14] A. Klein, S. Tiefenbacher, V. Eyert, C. Pettenkofer, W. Jaegermann, *Phys. Rev. B* **2001**, *64*, 205416.
[15] W. Zhao, Z. Ghorannevis, L. Chu, M. Toh, C. Kloc, P. H. Tan, G. Eda, *ACS Nano* **2013**, *7*, 791.
[16] H. Jiang, *J. Phys. Chem. C* **2012**, *116*, 7664.
[17] A. Chernikov, T. C. Berkelbach, H. M. Hill, A. Rigosi, Y. Li, O. B. Aslan, D. R. Reichman, M. S. Hybertsen, T. F. Heinz, *Phys. Rev. Lett.* **2014**, *113*, 076802.
[18] A. Ramasubramaniam, *Phys. Rev. B – Condens. Matter Mater. Phys.* **2012**, *86*, 115409.
[19] H. Shi, H. Pan, Y. W. Zhang, B. I. Yakobson, *Phys. Rev. B – Condens. Matter Mater. Phys.* **2013**, *87*, 155304.
[20] K. Keyshar, M. Berg, X. Zhang, R. Vajtai, G. Gupta, C. K. Chan, T. E. Beechem, P. M. Ajayan, A. D. Mohite, T. Ohta, *ACS Nano* **2017**, *11*, 8223.
[21] J. Kang, S. Tongay, J. Zhou, J. Li, J. Wu, *Appl. Phys. Lett.* **2013**, *102*, 012111.
[22] B. Zhu, X. Chen, X. Cui, *Sci. Rep.* **2015**, *5*, 9218.
[23] A. Splendiani, L. Sun, Y. Zhang, T. Li, J. Kim, C. Y. Chim, G. Galli, F. Wang, *Nano Lett.* **2010**, *10*, 1271.
[24] A. Kuc, N. Zibouche, T. Heine, *Phys. Rev. B – Condens. Matter Mater. Phys.* **2011**, *83*, 245213.
[25] W. Zhao, R. M. Ribeiro, M. Toh, A. Carvalho, C. Kloc, A. H. Castro Neto, G. Eda, *Nano Lett.* **2013**, *13*, 5627.
[26] M. R. Molas, K. Nogajewski, A. O. Slobodeniuk, J. Binder, M. Bartos, M. Potemski, *Nanoscale* **2017**, *9*, 13128.
[27] A. Arora, M. Koperski, K. Nogajewski, J. Marcus, C. Faugeras, M. Potemski, *Nanoscale* **2015**, *7*, 10421.
[28] W. S. Yun, S. W. Han, S. C. Hong, I. G. Kim, J. D. Lee, *Phys. Rev. B – Condens. Matter Mater. Phys.* **2012**, *85*, 033305.
[29] S. Tongay, J. Zhou, C. Ataca, K. Lo, T. S. Matthews, J. Li, J. C. Grossman, J. Wu, *Nano Lett.* **2012**, *12*, 5576.
[30] H. Jeong, G. H. Cho, J. Yoo, S. M. Lee, R. Salas-Montiel, H. Ko, K. K. Kim, M. S. Jeong, *Appl. Surf. Sci.* **2024**, *653*, 159382.
[31] A. Berkdemir, H. R. Gutiérrez, A. R. Botello-Méndez, N. Perea-López, A. L. Elías, C. I. Chia, B. Wang, V. H. Crespi, F. López-Urías, J. C. Charlier, H. Terrones, M. Terrones, *Sci. Rep.* **2013**, *3*, 1755.
[32] M. H. Naik, M. Jain, *Phys. Rev. B* **2017**, *95*, 165125.
[33] A. Katrib, F. Hemming, P. Wehrer, L. Hilaire, G. Maire, *Catal. Lett.* **1994**, *29*, 397.
[34] F. Liu, W. Wu, Y. Bai, S. H. Chae, Q. Li, J. Wang, J. Hone, X. Y. Zhu, *Science* **2020**, *367*, 903.